JSR Publications

Available Online

J. Sci. Res. **16** (1), 41-51 (2024)

JOURNAL OF SCIENTIFIC RESEARCH

www.banglajol.info/index.php/JSR

Effect of Different Compositions of Mixed Metal Oxides (Zinc Oxide and Tin Oxide) on Structural and Optical Properties for the Application of Window Layers in Solar Cells

A. Khandelwal*, R. Shukla, K. S. Sharma

Department of Physics, IIS (Deemed to be University), Gurukul Marg, Mansarover, Jaipur 302020, India

Received 26 January 2023, accepted in final revised form 5 August 2023

Abstract

Thin films of composite Zinc Tin Oxide (ZTO) are grown on glass substrates by thermal vapor evaporation. Thin films with different ratios of ZnO: SnO_2= (90:10, 80:20, 70:30, 60:40 and 50:50) wt% were prepared and annealed at 500 °C for 2 h. The X-ray diffraction (XRD) patterns reveal that the ZTO films have become polycrystalline as we increase the percentage of tin oxide. The crystallinity of films also increases significantly. The field emission scanning electron microscopy (FESEM) results indicate that the percentage of tin oxide changes the film's morphology. UV visible spectroscopy of the films indicates that the band gap is reduced with the increased percentage of tin oxide in the mixture, and transmittance is also decreased at a higher percentage. The transmittance of the films ranges from 90 to 83 %, while the band gap falls within the range of 3.90 to 3.40 eV. These characteristics make the films well-suited for solar cell window layers.

Keywords: Composite ZTO thin films; XRD; FESEM with EDAX; Optical band gap.

doi: http://dx.doi.org/10.3329/jsr.v16i1.64157 J. Sci. Res. **16** (1), 41-51 (2024)

1. Introduction

Transparent conducting oxides (TCOs) have numerous applications, including flat-panel displays, solar cells, gas sensors, and light-emitting diodes [1-7]. Because of their exceptional thermal and chemical stability, zinc-tin-oxide materials have recently gained much interest [1-5]. Because of their high mobility and good optical transmittance, zinc tin oxide (ZTO) films have recently been explored in favorable n-type conductivity material [8]. ZTO was discovered to have greater thermal and chemical stability than films of undoped tin oxide (SnO_2) and zinc oxide (ZnO) [9]. We selected Sn as the dopant because it transforms into Sn^{4+} when it takes the place of the Zn^{2+} spot in the ZnO crystal structure, resulting in two additional free electrons to facilitate electrical conduction [10]. Additionally, the radius difference between Sn^{4+} and Zn^{2+} is about 30 %; therefore, a restricted solid solution is attainable [11]. The existence of two crystal structures for ZTO is widely acknowledged. The first is $ZnSnO_3$, zinc metastannate, and the second is

* *Corresponding author*: akansha.khandelwal@iisuniv.ac.in

Zn_2SnO_4, zinc orthostannate. On the other hand, little is known about how composition and crystallinity relate. Due to the fact that ternary materials can be made from a variety of binaries with different crystal structures, densities, or stoichiometries, there is a dearth of knowledge regarding many other ternary oxides as well.

Cadmium sulphide (CdS) is frequently utilized as a buffer layer due to its low bandgap. Parasitic absorption occurs in low-wavelength lights. Its drawbacks include high cadmium toxicity and the non-vacuum method's incompatibility with the Copper Indium Gallium Selenide (CIGS) process. As a result, ZTO is promoted as a useful buffer layer to replace the use of CdS in solar cells. The band gap can be efficiently controlled, operated stably even at high temperatures, and exhibit high light transmittance by controlling the zinc and tin ratio. Furthermore, the non-toxicity of zinc and tin is a benefit. The desirable properties of CdS (with a wide energy band gap of 2.4 eV) and ZnS (with a wide energy band gap of 3.4 eV) make them excellent materials for window applications. The use of CdS thin films as window layers in heterojunction devices may lead to environmental concerns due to the material's toxicity, which is attributed to its instability in the air [12]. To offer a viable substitute for CdS thin films, we synthesized ZTO thin films.

Sputtering [13-16] is commonly used to deposit ZTO films, but other methods, such as pulsed laser deposition (PLD) [17], filtered vacuum arc [18], and flash evaporation [19], have also been explored. Thin films of ZnO and SnO_2 have been synthesized by thermal evaporation, and post-deposition annealing has been employed to enhance their optical characteristics [20,21]. Sometimes, depositing ZTO films in a thermal evaporator would be advantageous. ZTO may be employed as the cathode or electron transport layer in several organic and hybrid devices [4,5]. And it is a cost-effective technique also. Therefore, the entire device structure can be created in one system without compromising the vacuum if the ZTO layer is deposited using the thermal evaporation technique.

In this work, we have taken five different ratios of Zinc Oxide and Tin Oxide so that we can find out how the properties (especially band gap and transmittance) of ZTO can be useful for the application of the window layer of solar cells. The effect of different compositions with different ratios of ZnO and SnO_2 on the properties of ZTO thin films deposited by Thermal vapor evaporation has been investigated using X-ray diffraction (XRD), Field emission scanning electron microscopy (FESEM) with Energy Dispersive X-ray Analysis (EDAX) and UV-Vis spectrophotometer. The current study aims to identify the impact of various ZnO and SnO_2 compositions on the structural, morphological, and optical properties of ZTO films prepared on glass substrates. The mechanism of compositional influence on the property was also thoroughly discussed.

2. Materials and Methods

ZnO and SnO_2 in powder form with 99.9 % purity were obtained from Sigma Aldrich (USA). Thermal vacuum evaporation is used to develop ZTO thin films of different ratios of Zinc Oxide and Tin Oxide on glass substrates by using a HINDHI vacuum coating set-

up (Smart Coat 3.0 A Thermal Evaporation System, Hind High Vacuum Co. Pvt. Ltd., Bangalore) with a molecular turbo pump maintaining the pressure of 10^{-6} torr.

2.1. *Experimental details*

2.1.1. *Substrate cleaning*

We are taking glass as a substrate for our films. First of all, we cleaned the substrate with deionized water. Later it was treated with acetone and ethanol for 15 min, respectively, and lastly, sonicated at 100 °C for 30 min. Proper substrate cleaning is necessary to avoid impurities and achieve good-quality films**.**

2.1.2. *Preparation of ZTO thin films*

A mortar and pestle were used to mix ZnO and SnO_2 powders with 99.9 % purity at different concentrations (90:10, 80:20,70:30,60:40, and 50:50 wt.%) for about 5 hours. A molybdenum boat was inserted into the HINDHI vacuum coating unit to hold this mixture. The target and source were set apart by a fixed 10 cm. A. The thickness of the developed films was measured using a quartz crystal thickness monitor. The measured thickness ranged from 100 to 200 nm for the prepared films. For uniform deposition of composite (ZTO) thin films, the experimental conditions were not altered. The films were then annealed in a muffle furnace at 500 °C for 2 h to obtain crystalline ZTO films. This is the optimum temperature for annealing films because films begin to degrade above this temperature.

2.2. Characterizations

The crystallinity of films was examined by employing an X-ray diffractometer (Bruker Lynx Eye detector) using Cu-Kα radiation (0.154 nm). The optical properties of the ZTO films were studied in the wavelength range 300-800 nm using a UV-vis- near-infrared spectrometer (Perkin Elmer, Lambda 750, USA). The film's surface morphology was imaged using Nova Nano FE-SEM 450 (FEI) Model Scanning Electron Microscope (FESEM with EDAX).

3. Results and Discussion

3.1 *Structural Analysis*

The obtained XRD pattern of ZTO thin films is shown in Fig. 1. From the analysis, it has been found that the films are polycrystalline in nature. One peak appeared at 2θ=23.14° (JCPDS file=00-052-1381) with desired orientation along (012) plane of ZTO ($ZnSnO_3$) with rhombohedral structure (a=0.528 nm and c=1.409 nm). Meanwhile, two more peaks have appeared at 2θ=31.23° (JCPDS file=00-029-1484) at the plane (020) and 28.6°

(JCPDS file=00-021-1486) respectively for SnO_2 and ZnO for all five samples. Some new peaks also appeared as the concentration of SnO_2 increased. These peaks might be the result of the formation of earlier reported compounds like (ZnO)1-x (SnO_2)x [22,23], and some are due to defects that arise in structure with the increase in the ratio of SnO_2.

The crystallite size was calculated by Debye Scherer's equation for different Compositions [24].

$$D = \frac{0.9\lambda}{\beta cos\theta} \quad (1)$$

Where D is the average Crystallite size, λ is the wavelength of X-rays, β is the full-width half maxima, and θ is the angle of diffraction. The increment in grain size can be attributed to the improvement of crystallinity with the increasing percentage of SnO_2. It was found that crystallite size enhanced with improving the percentage of SnO_2, and surface adatom mobility of the species increased, leading to a coalition of smaller grains [19]. The calculated crystallite size values for different ratios of ZnO and SnO_2 thin films are presented in Table 1. The above findings are in conformity with the findings reported recently [19,25]. We can say that crystalline cell growth occurs due to the inclusion of SnO_2 in the ZnO structure. This expansion occurs due to the various atomic ratios, as the Sn atomic ratio is greater than the Zn atomic ratio. The results show that Sn atoms have an interstitial influence on Zn atoms.

We may estimate the dislocation density (δ) and lattice strain of ZTO thin films using the following relationship based on the present structural investigations [27]:

$$\delta = \frac{n}{D^2} \quad (2)$$

Where n = 1, always indicates the minimum dislocation density of the film, and D is the crystallite size. Any material's dislocation density reveals the defect structure and film quality. Dislocation density describes the number of dislocations per unit length or per unit area [26,28].

Table 1. Calculated structure parameters of composite ZTO thin films.

Different ratios of ZnO and SnO_2	FWHM	Crystallite size(nm)	Dislocation density	Lattice Strain
90:10	0.7051	15.33	4.255×10^{-3}	1.124×10^{-3}
80:20	0.4178	19.62	2.597×10^{-3}	0.466×10^{-3}
70:30	0.38275	21.43	2.177×10^{-3}	0.367×10^{-3}
60:40	0.38853	22.00	2.066×10^{-3}	0.446×10^{-3}
50:50	0.30764	27.18	1.353×10^{-3}	0.347×10^{-3}

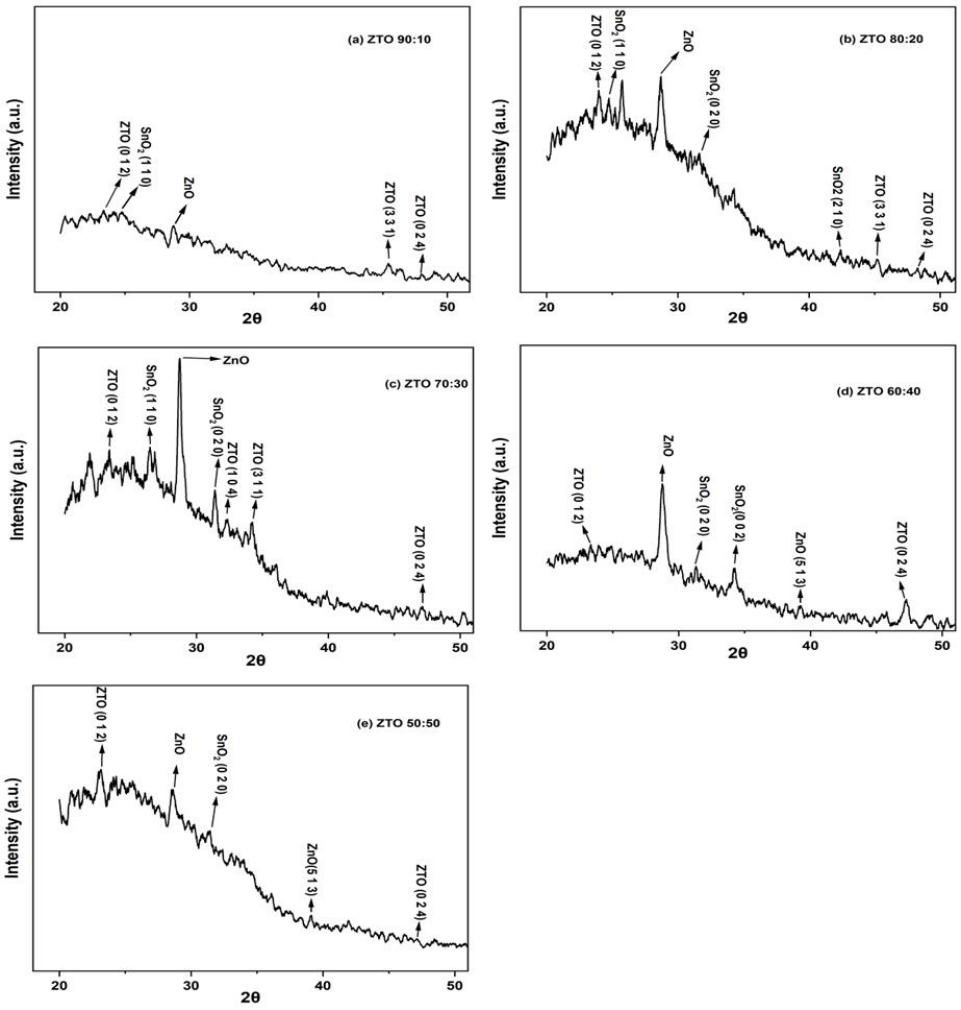

Fig. 1. XRD profile of composite ZTO thin films. (a) ZTO (90:10), (b) ZTO (80:20), (c) ZTO (70:30), and (d) ZTO (60:40), and (e) ZTO (50:50).

3.2. *Morphological analysis*

FESEM micrographs of ZTO thin films at x20K magnification are shown in Fig. 2. Field emission scanning electron microscopy (FESEM) was used to analyze the film's surface morphology of deposited thin films. The different ratios of ZnO and SnO_2 modify the film morphology, as seen in FESEM micrographs. After increasing the percentage of SnO_2, thin film surfaces presented many irregular and particle-like grains [29], and a change in shape was also observed. It changes from a flake-like structure to a petal-like structure with respect to an increment in the percentage of SnO_2 [30]. Grain size also increased with

the increase of SnO_2, which is evident from the FESEM pictures and in agreement with XRD results.

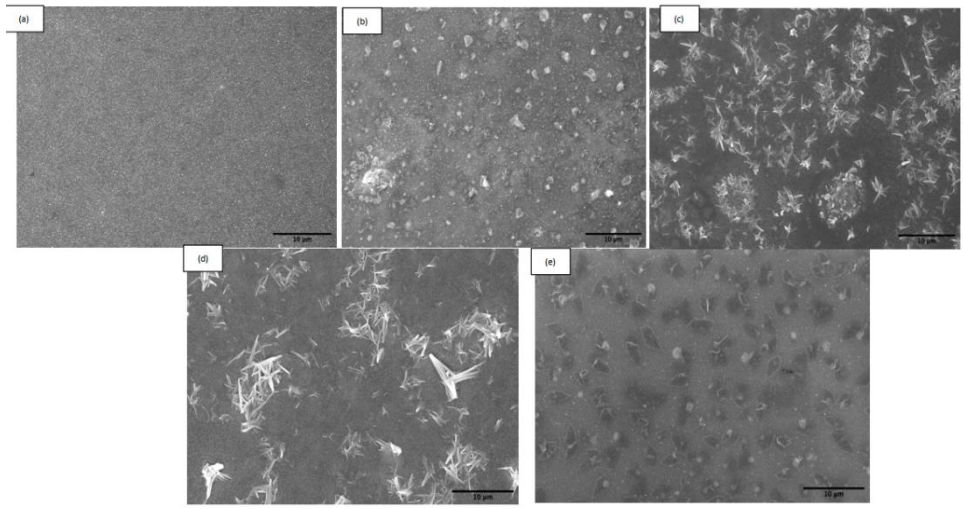

Fig. 2. FESEM images of composite ZTO thin films. (a) ZTO (90:10), (b) ZTO (80:20), (c) ZTO (70:30), and (d) ZTO (60:40), and (e) ZTO (50:50).

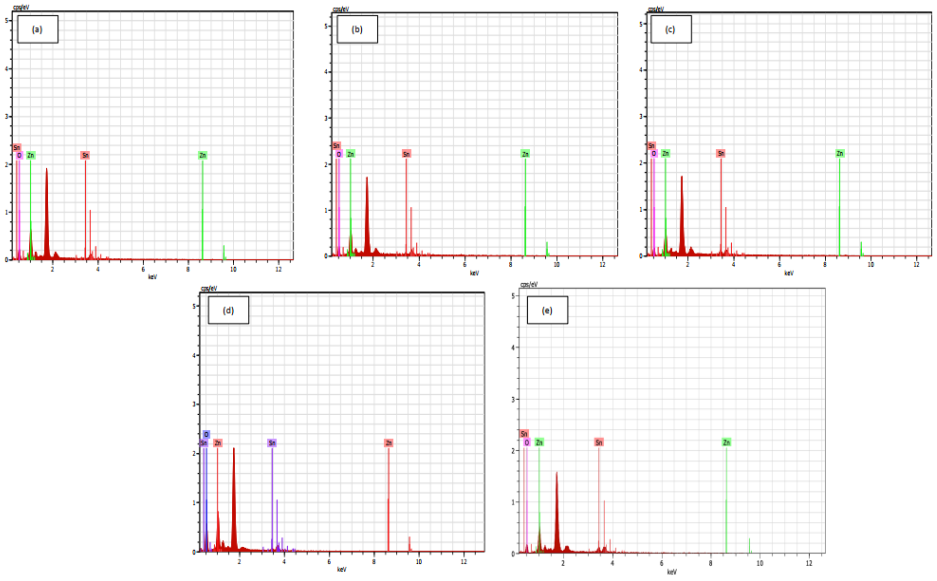

Fig. 3. EDAX image of composite ZTO thin films. (a) ZTO (90:10), (b) ZTO (80:20), (c) ZTO (70:30), and (d) ZTO (60:40), and (e) ZTO (50:50).

The zinc (Zn), tin (Sn), and oxygen (O) elemental compositions are analyzed by EDAX spectra (Fig. 3) at different locations of each sample. The composition is justified for all five samples, which is incorporated in Table 2.

Table 2. Elemental composition of ZTO thin films for all five ratios.

Film Type	% Composition		
	Zinc	Tin	Oxygen
90:10	39.38	5.95	54.67
80:20	22.52	6.29	71.19
70:30	37.27	10.76	51.97
60:40	41.65	11.87	46.48
50:50	37.78	12.78	49.44

3.3. *Optical analysis*

The energy gaps were calculated with the help of absorbance spectra for direct transitions. These values are determined by plotting $(\alpha h\nu)^2$ against $h\nu^2$. Fig. 4 explains the change in the band gap (Eg) values of ZnO thin films as the SnO_2 percentage increases. The band gap energies are found to range from a high of 3.90 eV for 10 % SnO_2 to a low of 3.40 eV at 50% SnO_2. The general trend reported is band gap narrowing, which means that the value of E_g diminished as tin concentration increased. This reduction in Band gap values might be attributed to the electronic states produced by defects in the material caused by SnO_2 inclusion [30]. The Fig clearly shows that the optical band gap decreases with increasing SnO_2%, which may be ascribed to an increase in carrier density, which results in the occupation of lower states in the conduction band [19].

The optical transmittance of ZTO thin films was obtained by using a UV-VIS spectrophotometer. For a higher percentage of SnO_2, the transmittance reduces. There is an abrupt absorption edge for all atomic content of SnO_2 into ZnO, which corresponds to a material with a direct energy gap [30]. As SnO_2 increases, this absorption edge shifts towards the left. A similar trend for absorption spectra is also seen. Electronic states most likely cause the reduction in transmittance within the ZnO bandgap, which produces a drop in Eg. [30].

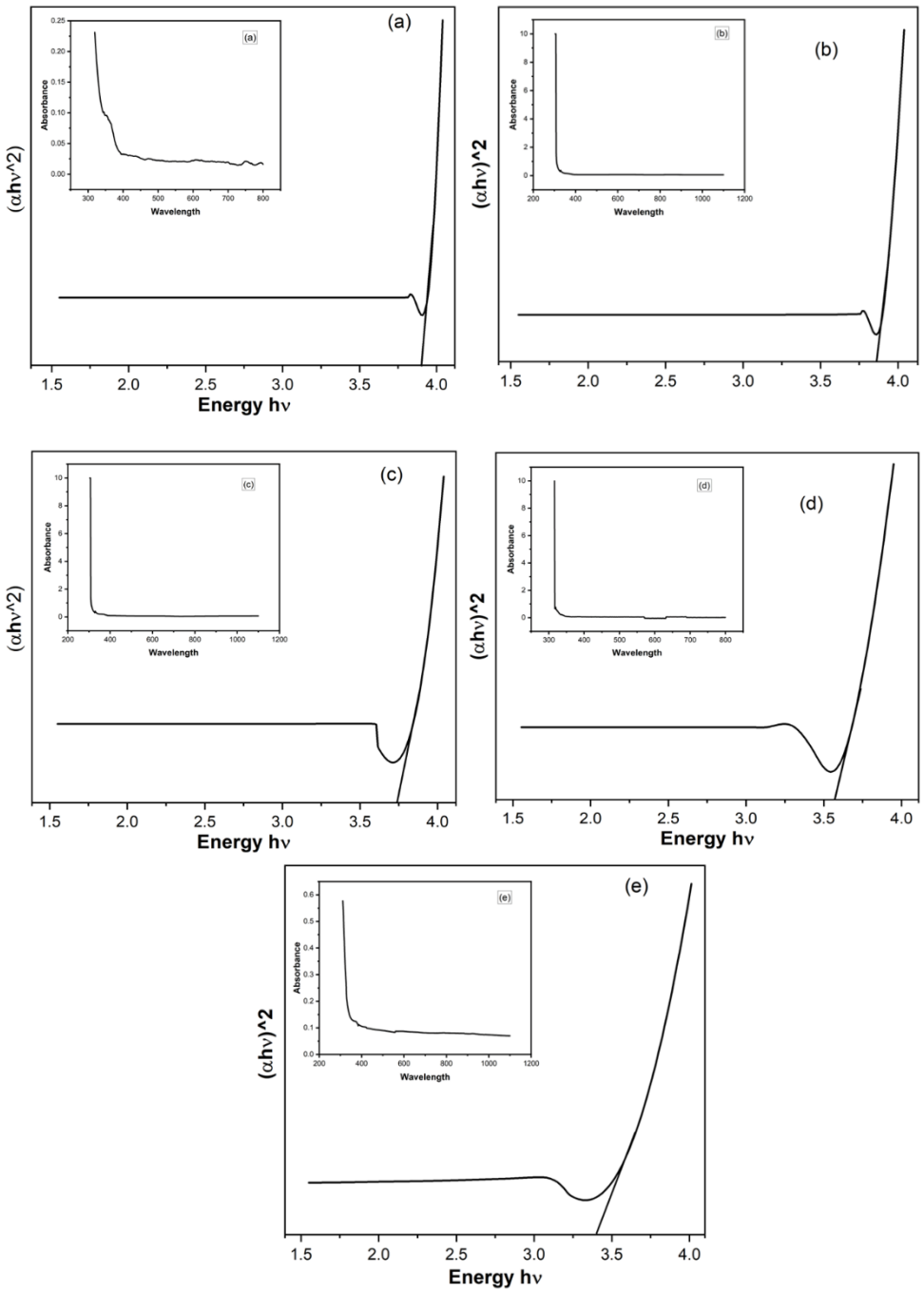

Fig. 4. The optical band gap of composite ZTO thin films. (a) ZTO (90:10), (b) ZTO (80:20), (c) ZTO (70:30), (d) ZTO (60:40), and (e) ZTO (50:50).

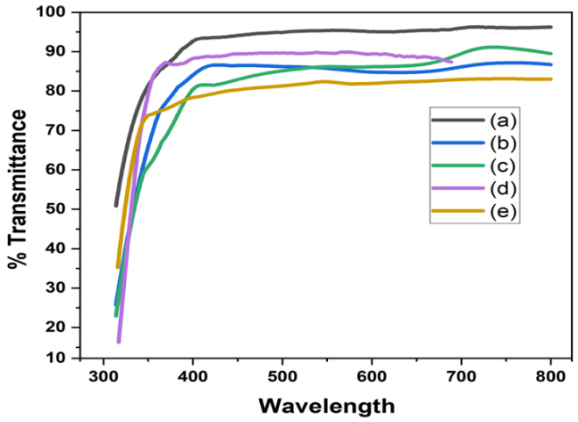

Fig. 5. Transmission spectra of composite ZTO thin film. (a) ZTO (90:10), (b) ZTO (80:20), (c) ZTO (70:30), (d) ZTO (60:40), and (e) ZTO (50:50).

Table 3. Optical band gap of ZTO thin films.

S. No.	Different ratios of ZnO and SnO_2	Band gap
1.	90:10	3.90 eV
2	80:20	3.86 eV
3	70:30	3.73 eV
4	60:40	3.57 eV
5	50:50	3.40 eV

4. Conclusion

The thin films of ZnO and SnO_2 prepared successfully by thermal vacuum evaporation have been prepared successfully. The XRD results indicate that films become polycrystalline when the percentage of SnO_2 increases in ZnO. Crystallite size also increases with the increase of SnO_2 percentage. FESEM reveals that the increase in the percentage of Tin oxide changes the morphology of the films. As the Percentage of Tin oxide in the mixture increases, the concentration of Zn on the surface of the film decreases, but the opposite is true for Tin which is very evident in EDAX results. The optical band gap of the composite ZTO thin films decreases by increasing the Percentage of SnO_2 in ZnO. The transmittance also decreases for a higher percentage of SnO_2. But the transmittance value is between 90-83 %, which is a good range for using ZTO films in applications like window layers in solar cells.

Acknowledgment

One of the authors (A. Khandelwal) would like to show her gratitude to Material Research Centre (MRC), MNIT, Jaipur, for providing her with the research facilities and the required technical assistance during the characterization of her films.

References

1. D. S. Ginley and C. Bright, MRS Bull. **25**, 15 (2000). https://doi.org/10.1557/mrs2000.256
2. A. Khandelwal, R. Shukla, and K. S**.** Sharma, Neuro Quantol. **20**, 2932 (2022).
3. J. H. Yu and G. M. Choi, Sens. Actuators B **72**, 141 (2001).
4. K. L. Chopra, P. D. Paulson, and V. Dutta, Res. Appl. **12**, 69 (2004). https://doi.org/10.1002/pip.541
5. P. Görrn, M. Sander, J. Meyer, M. Kröger, et al., Adv. Mater. **18**, 738 (2006). https://doi.org/10.1002/adma.200501957
6. V. Wood, M. J. Panzer, J. E. Halpert, J. M. Caruge, M. G. Bawendi, and V. Bulovic, ACS Nano **3**, 3581 (2009). https://doi.org/10.1021/nn901074r
7. H. Guo, H. B Andagana, and X. A. Cao, J. Electron. Mater. **39**, 494 (2010). https://doi.org/10.1007/s11664-010-1133-4
8. H. Q. Chiang, J. F. Wager, and R. L. Hoffman, Appl. Phys. Lett. **86**, ID 013503 (2005). https://doi.org/10.1063/1.1843286
9. T. Minami, S. Takata, and H. Sato, J. Vac. Sci. Technol. A **13**, 1095 (1995). https://doi.org/10.1116/1.579592
10. S. Roguai and A. Djelloul, Solid State Commun. **350**, 114740 (2022). https://doi.org/10.1016/j.ssc.2022.114740
11. M. Ajili, M. Castagne, and N. K. Turki, Superlattices Microstruct. **53**, 213 (2013). https://doi.org/10.1016/j. spmi.2012.10.012
12. V. A. Owoeye, E. Ajenifuja, A. E. Adeoye, A. O. Salau, et al., ERX **3**, ID 025012 (2021). https://doi.org/10.1088/2631-8695/abf65f
13. T. Minami, H. Sonohara, S. Takata, and H. Sato, Jpn. J. Appl. Phys. **33**, ID L1693 (1994). https://doi.org/10.1143/JJAP.33.L1693
14. D. L. Young, H. Moutinho, Y. Yan and T. J. Coutts, J. Appl. Phys. **92**, 310 (2002). https://doi.org/10.1063/1.1483104
15. T. Moriga, Y. Hayashi, K. Kondo, Y. Nishimura, et al., J. Vac. Sci. Technol. A **22**, 1705 (2004). https://doi.org/10.1116/1.1765658
16. J. H. Ko, I. H. Kim, D. Kim, K. S. Lee, *et al*., Appl. Surf. Sci. **253**, 7398 (2007). https://doi.org/10.1016/j.apsusc.2007.03.036
17. M. K. Jayaraj, K. J. Saji, K. Nomura, T. Kamiya, and H. Hosono, J. Vac. Sci. Technol. B **26**, 495 (2008). https://doi.org/10.1116/1.2839860
18. E. Çetinörgü, S. Goldsmith, and R. L. Boxman, Thin Solid Films **515**, 880 (2006). https://doi.org/10.1016/j.tsf.2006.07.050
19. V. K. Jain, P. Kumar, M. Kumar, P. Jain, D. Bhandari, and Y. K. Vijay, J. Alloys Compd. **509**, 3541 (2011). https://doi.org/10.1016/j.jallcom.2010.10.212
20. D. W. Lane, J. A. Coath, K. D. Rogers, B. J. Hunnikin, and H. S. Beldon, Thin Solid Films **221**, 262 (1992). https://doi.org/10.1016/0040-6090(92)90824-U
21. N. Bouhssira, S. Abed, E. Tomasella, J. Cellier, et al., Appl. Surf. Sci. **252**, 5594 https://doi.org/10.1016/j.apsusc.2005.12.134
22. J. H. Ko, I. H. Kim, D. Kim, K. S. Lee, *et al.*, Appl. Surf. Sci. **253**, 7398 (2007). https://doi.org/10.1016/j.apsusc.2007.03.036
23. W. J. Moon, J. H. Yu, and G. M. Choi, Sens. Actuators B **80**, 21 (2001). https://doi.org/10.1016/S0925-4005(01)00884-X
24. A. Khandelwal, R. Shukla, J. Gangwar, and K. S. Sharma, J. Sc. Tech. **10**, 65 (2021).
25. V. Ganesh, I. S. Yahia, S. AlFaify, and M. Shkir, J. Phys. Chem. Solids **100**, 115 (2017). http://dx.doi.org/10.1016/j.jpcs.2016.09.022
26. M. Miki-Yoshida, J. Morales, and J. Solis,Thin Solid Films **373**, 137 (2000). https://doi.org/10.1016/S0040-6090(00)01120-2
27. K. Usha, R. Sivakumar, and C. Sanjeeviraja, J. Appl. Phys. **114**, 123501 (2013). https://doi.org/10.1063/1.4821966
28. S. Saha and V. Gupta, AIP Adv. **1**, ID 042112 (2011). https://doi.org/10.1063/1.3654497

29. K. J. Chen, F.Y. Hung, Y.T. Chen, S. J. Chang, and Z. S. Hu, Mater. Trans. **51**, 1340 (2010). https://doi.org/10.2320/matertrans.M2009378
30. J. A. Berumen-Torres, J. G. Quinones-Galvan, H. Duran-Munoz, C. H. Guzman, et al., Mater. Sci. Eng B **268**, ID 115134 (2021). https://doi.org/10.1016/j.mseb.2021.115134